JMEPEG (2001) 10:371–377

Stress Corrosion Cracking of A588 Steel Weldments in Flue Gas Related Environments

L.W. Tsay, W.Y. Chen, R.K. Shiue, and R.H. Shiue

(Submitted 2 May 2000; in revised form 28 August 2000)

This study investigated stress corrosion cracking (SCC) of A588 steel welds as determined by U-bend immersion tests and slow strain rate tensile (SSRT) tests to evaluate the steel's cracking susceptibility in various regions of the weldments. The immersion test results indicated that the fusion zone (FZ) had better corrosion resistance than the other regions in the weld. It was also demonstrated that the columnar grain boundaries exhibited a higher resistance to corrosion than the grain interior of the FZ. However, the coarse elongated ferrite in the FZ is susceptible to hydrogen embrittlement (HE), which results in the formation of microcracks. As a result, a severe degradation of the weld's tensile properties in the saturated H_2S solution was observed. Scanning electron microscope (SEM) fractographs of tensile specimens reveal a cleavage fracture in the coarse-grained heat-affected zone (CGHAZ) and featherlike rupture in the FZ, both indicating a high sensitivity to HE.

Keywords hydrogen embrittlement, overlay welding, repair welding, slow strain rate tensile test, stress corrosion cracking, U-bend test

1. Introduction

The combustion of pulverized coal generates aggressive chemical atmospheres containing H_2, H_2S, CO_2, and SO_2, which can cause flue gas duct and its accessories stress corrosion cracking (SCC). The flue gas duct is usually constructed of welded A588 weathering steel. The addition of a minor amount of copper into carbon steels results in the formation of a dense oxide layer on the steel surface that prevents the metal from continued oxidation.[1,2] Thus, the corrosion resistance of A588 steel is higher than that of both plain carbon and high-strength low-alloy steels.[1–4] In addition, alloying elements such as Cu, Ni, and Cr in A588 steel have been found to increase pitting resistance of the steel.[5] Therefore, A588 steel is widely used without coating as the construction material in atmospheric corrosion environments.[6–8]

Although the hardenability of A588 steel is slightly higher than that of low-alloy C-Mn steel, it can be welded through careful control of welding procedures to prevent hydrogen-induced cracking in the heat-affected zone (HAZ).[9,10] The HAZ in A588 steel exhibits acceptable strength and toughness over a wide range of welding heat inputs in the as-welded condition.[10] Postweld heat treatment at 620 °C/10 h of this type of weld has a limited effect on its strength but provides increased transition temperature of the HAZ.[11]

U-bend[12,13,14] and slow strain rate tensile (SSRT) tests[15–18] are widely used to evaluate the susceptibility to SCC of various materials. A short incubation time will be produced if a large strain can be imposed on the experimental specimens during U-bend tests. With the SSRT test, the specimen is generally strained to failure. However, in this method, the test condition might exceed the actual service condition because of the high stress state generated at the crack tip.[15] Also, the strain rate plays an important role in the material/environment system. Different fracture mechanisms may be dominant at different strain rates. It has been demonstrated that SSRT is advantageous in shortening the evaluation time,[15–19] but there is still a discrepancy from the realistic loading and environmental conditions.

Various aqueous solutions including sulfuric acid solution and hydrogen sulfide solution may damage the construction of flue gas ducts during service. In addition, the presence of residual stresses in the weldment promotes the occurrence of SCC of the welds. In general, high-strength steel welds are susceptible to hydrogen embrittlement (HE), of which sulfide stress corrosion cracking (SSCC) is a typical example.[20,21]

The objective of the current study was to examine the susceptibility of repair welds (RWs) and overlay welds (OWs) to SCC in sulfuric acid and hydrogen sulfide environments.

2. Experimental Procedures

2.1 Specimen Preparation

The material used in this study was A588 weathering steel plate of 15 mm thickness. The chemical composition of the steel in weight percent was 0.1C, 0.29Si, 1.35Mn, 0.015P, 0.004S, 0.14Ni, 0.25Cu, 0.024Nb, 0.4Cr, and balance Fe. Two types of welded specimens, RWs and OWs, were made using the shielded metal arc welding (SMAW) process. Schematic diagrams showing the joint geometry of the welds and the dimensions of the U-bend specimen sectioned from the welds are shown in Fig. 1. The RW specimen has a 90° single V groove of 6 mm depth and 4 mm root radius (Fig. 1a). Two welding passes were necessary to fill the joint. The joint design of the

L.W. Tsay, Institute of Materials Engineering, National Taiwan Ocean University, Keelung 202, Taiwan, Republic of China; **W.Y. Chen** and **R.K. Shiue,** Institute of Materials Science and Engineering, National Dong Hwa University, Hualien 974, Taiwan, Republic of China; and **R.H. Shiue,** Boiler Division, Taiwan Power Company, Taichung 434, Taiwan, Republic of China. Contact e-mail: B0186@mail.ntou.edu.tw.

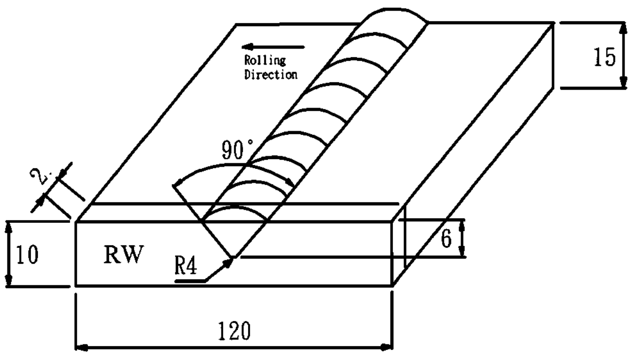

(**a**)

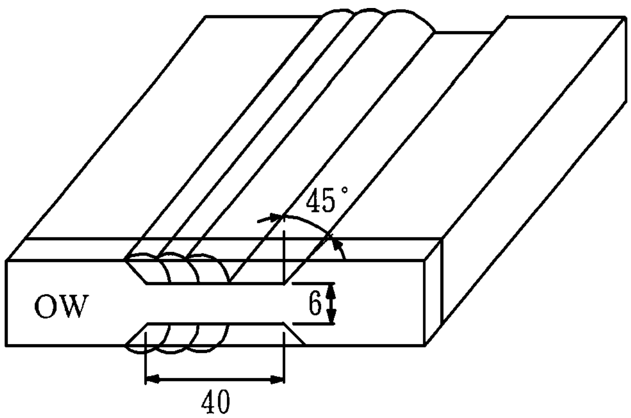

(**b**)

Fig. 1 Schematic diagrams showing the joint geometry of the (**a**) RW and (**b**) OW specimens and the dimensions of the U-bend specimen sectioned from the welds

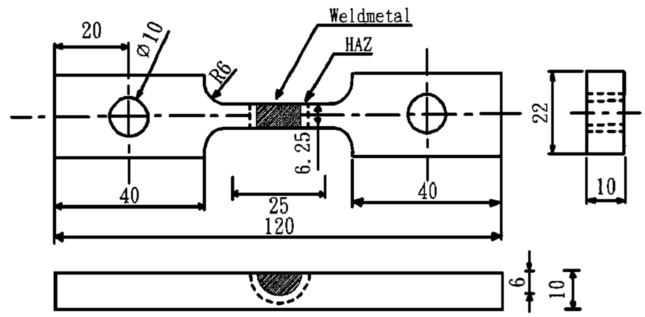

(**a**)

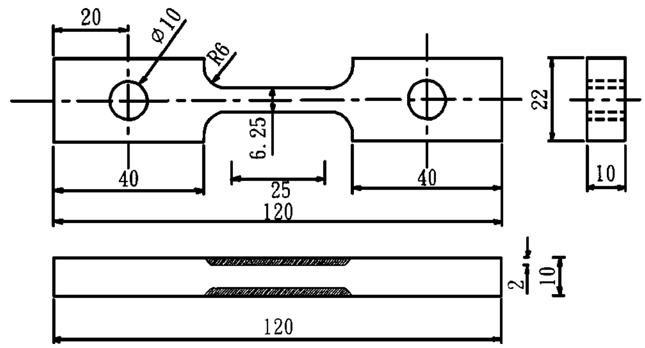

(**b**)

Fig. 2 Schematic diagrams showing the tensile specimen dimensions of (**a**) RW and (**b**) OW specimens

OW specimens, used to reduce welding distortion and to evaluate the properties of the surfacing welds, is shown in Fig. 1(b). The thickness of the overlay for each welding pass was about 3 mm. In order to complete the surfacing weld, 14 welding passes were necessary to cover the area of the surfacing groove on each face. AWS E8018-W electrodes of 4.0 mm in diameter were used in this study. The nominal composition of the electrodes in weight percent was 0.06C, 0.54Si, 0.84Mn, 0.014P, 0.009S, 0.61Ni, 0.48Cu, 0.52Cr, and balance Fe. Neither preheat nor postweld heat treatment of the welds was conducted.

2.2 Immersion Test

The dimensions of the U-bend specimen are 120 mm length × 10 mm width × 2 mm thickness. After deformation by a forming mold with a radius of 20 mm, the measured plastic strain of the released U-bend specimen was about 4.7%. The designed fixture was employed to maintain the plastic strain on the U-bend specimen during the immersion test. U-bend specimens were then immersed in the 1 and 0.5 N sulfuric acid solutions, as well as in the saturated H_2S solution.

2.3 Tensile Test

The dimensions of tensile specimens, with a gage length of 25 mm, are shown in Fig. 2. The weld bead is located at the center of the gage length of the RW specimen (Fig. 2a). The thickness of weld overlays on opposite sides of the tensile specimen was 2 mm after fabrication, as indicated in Fig. 2(b). Ordinary tensile tests were first conducted in air at room temperature at the strain rate of 5×10^{-4} s^{-1}. The SSRT tests were carried out at room temperature with a slower constant strain rate of 5×10^{-6} s^{-1} in a saturated H_2S solution. The test solution was prepared according to the NACE TM-01-77/86 standard. All tensile results are the average of at least three runs for each testing condition.

2.4 Microhardness Measurements and Metallographic Observations

Microhardness measurements across the fusion boundary were carried out using a Vickers microhardness tester. Three percent Nital etching solution was used to reveal the microstructures in various regions of the welds, which were then inspected by optical microscope. U-bend and tensile-fractured specimens were examined by scanning electron microscope (SEM) to reveal the fracture features of the crack-initiation sites.

3. Results and Discussion

3.1 Hardness Measurements and Metallographic Observation

Figure 3 shows the metallographs of RW and OW specimens with microhardness distribution in the as-welded condition, in which the HAZ was approximately 2 mm wide. As shown in

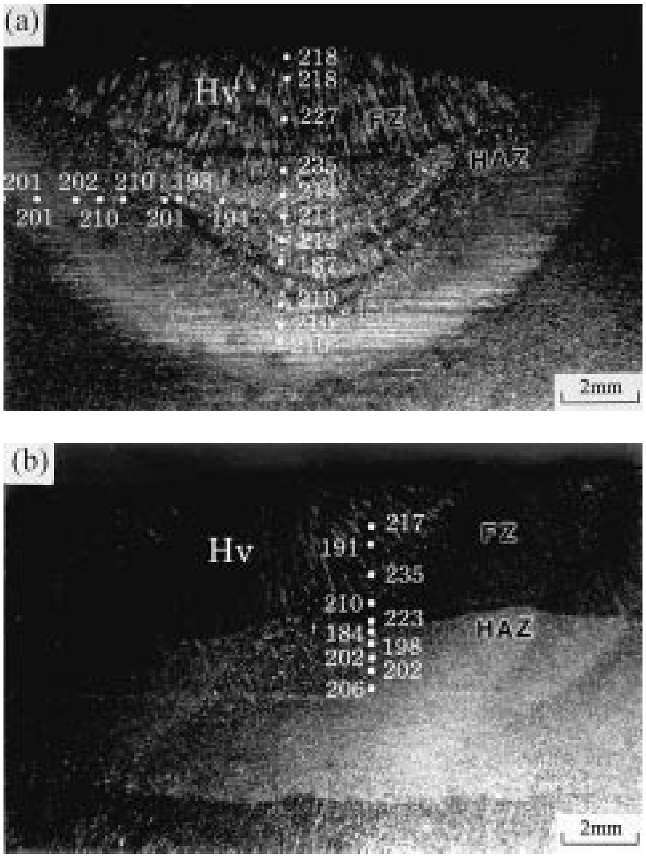

Fig. 3 Typical macrographs showing the microhardness distribution of (**a**) RW and (**b**) OW specimens

Fig. 3(a), the weld bead of the first pass was refined by a subsequent welding thermal cycle. The weld deposit of the final pass on the RW specimen was comprised of coarse columnar grains. Similarly, the presence of columnar grains could also be observed in the OW specimen. In multipass welding, the microstructures formed in the previous thermal cycle are tempered or refined by the subsequent welding passes, depending on the associated thermal history. At regions with a reheated peak temperature exceeding the Ac_3, hardened microstructures similar to that in the coarse-grained heat-affected zone (CGHAZ) of the initial weld pass are obtained. If the peak temperature is below Ac_1, only tempered microstructures are observed. As a result, the microhardness in the fusion zone (FZ) and/or HAZ showed certain fluctuations because of the variations in microstructures. Because of the low carbon equivalent of the welds, no obvious increase in hardness in the FZ and CGHAZ was found. The average hardness in the FZ was slightly higher than that in the other regions of the welds. The highest hardness was located in the junction between two welding deposits in the FZ with a microhardness of about Hv 235.

Metallographs of distinct regions in the weld are shown in Fig. 4, where the microstructures of the base metal (BM) consist of fine-grained ferrite and pearlite. In the region adjacent to the fusion boundary, much higher heating temperature was experienced. Thus, the coarse-grained austenite was mostly transformed into grain boundary ferrite, Widmanstätten side plates, and a few microphases (Fig. 4a). In the FZ, the coarse solidified microstructures were composed of elongated grain boundary ferrite, Widmanstätten ferrite, acicular ferrite, and a few microphases (Fig. 4b). The microstructure of the as-welded deposit was refined by subsequent welding thermal cycles. The effective reduction of coarse elongated ferrite and Widmanstätten side plates due to dynamic recrystallization could also be observed, as shown in Fig. 4(c).

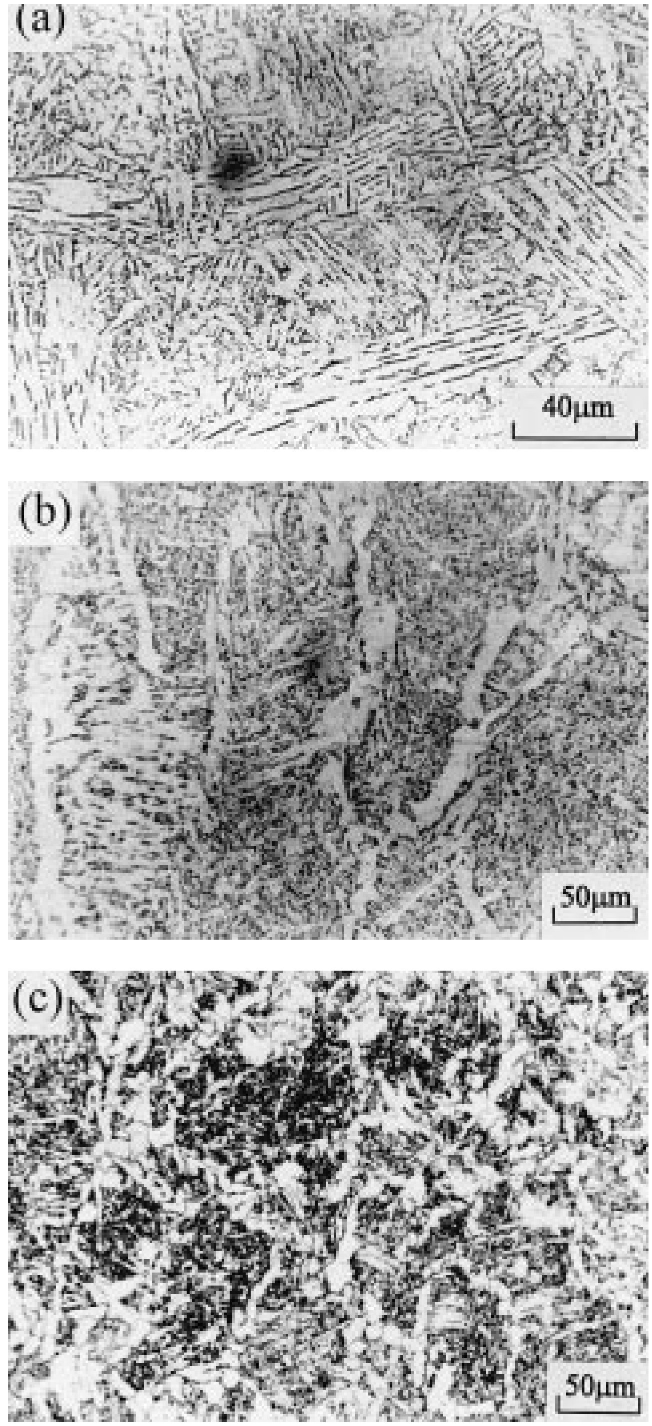

Fig. 4 Metallographs showing the (**a**) CGHAZ, (**b**) FZ, and (**c**) refined FZ in a RW weld

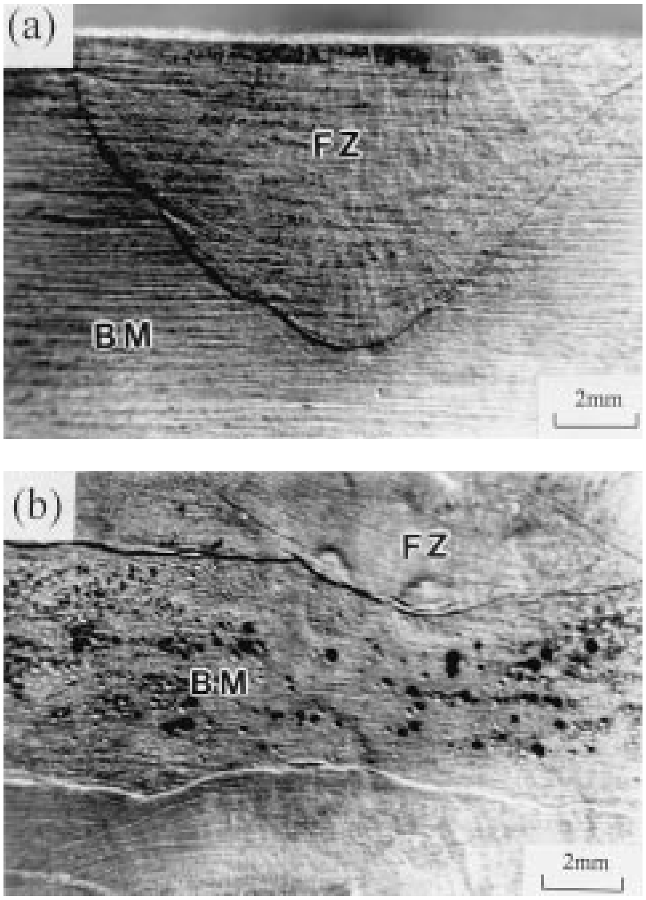

Fig. 5 Optical photographs of (**a**) RW and (**b**) OW specimens after U-bend tests in 0.5 N sulfuric acid solution for 15 h

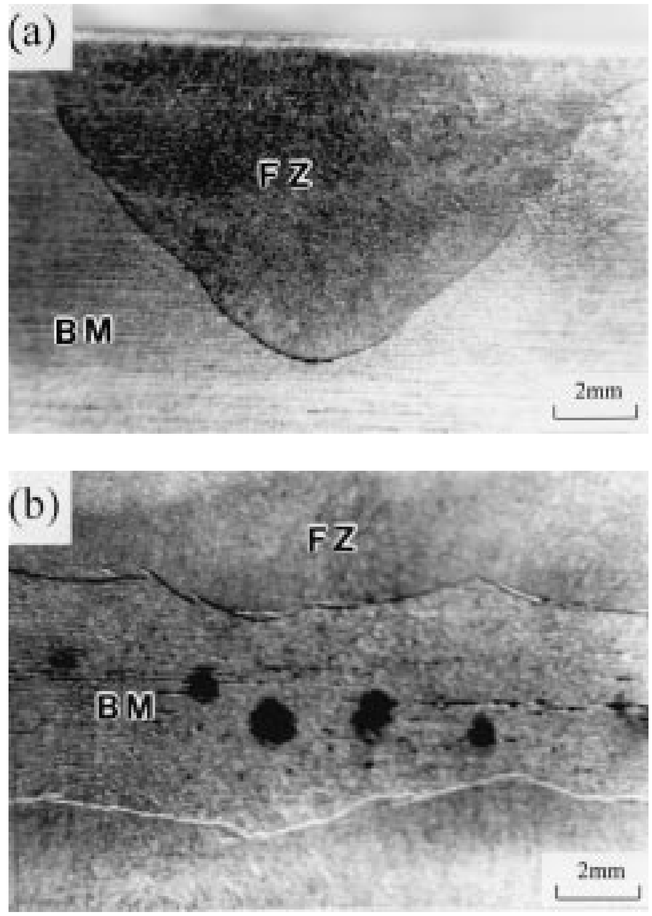

Fig. 6 Optical photographs of (**a**) RW and (**b**) OW specimens after U-bend tests in a saturated H_2S solution for 72 h

Table 1 Tensile properties of various specimens tested in air and in a saturated H_2S solution

	A588 steel plate		*RW specimen		**OW specimen	
Materials Properties/Condition	**In air**	**In H_2S**	**In air**	**In H_2S**	**In air**	**In H_2S**
***UTS (MPa)	605	603	607	580	642	515
Elongation (%)	32	12	32	9	30	7
Reduction in area (%)	65	14	64	8	61	4
Fracture location	BM	BM	BM	FZ	…	…

*RW: repair weld
**OW: overlay weld
***UTS: ultimate tensile strength

3.2 Immersion Test

The U-bend specimens, after immersion in 1 N sulfuric acid solution for 15 h, were seriously corroded and pitted. To highlight the difference in corrosion resistance between the FZ and the BM, a further reduction of the test solution concentration to 0.5 N was performed. Macroscopic photographs of the U-bend specimens immersed in 0.5 N sulfuric acid for 15 h are shown in Fig. 5, revealing that the FZ exhibits a higher corrosion resistance than the BM. The pitting corrosion in the BM is much more prominent than that in the FZ. The OW specimen was comprised of deposits 2 mm thick on the top and bottom surfaces, sandwiching an interior BM 6 mm thick. Due to the presence of a relatively small anodic region (BM) in the OW specimen, the degree of pitting corrosion in the BM of the OW specimen was much more prominent than that in the RW specimen, as demonstrated in Fig. 5(b). The results also indicate that A588 steel weldments are not susceptible to SCC in sulfuric acid solution.

The surface morphology of the A588 steel plate immersed in a saturated H_2S solution was examined. Specimens sectioned along the rolling direction from the steel plate (L section) presented a more severely banded structure than specimens sectioned in the direction transverse to the rolling direction (T section). After immersion in a H_2S solution for 24 h, the more prominently elongated MnS in the sample resulted in much poorer corrosion properties. After increasing the immersion time, microcracks along the aligned MnS inclusion became longer and corrosion pits became larger (results not shown). This is in accordance with Yamaguchi,[17] who indicated that hydrogen was trapped at the MnS site and crack initiation occurred when hydrogen concentration became high. The presence of elongated MnS inclusion along the rolling direction demonstrates that the L section was more susceptible to HE than the T section. Optical photographs of the RW and OW U-bend specimens after immersion in a saturated H_2S solution for 72 h are shown in Fig. 6. It can be seen that the corrosion resistance of the FZ was still better than that of the BM for differently processed specimens. Similarly, the BM in the OW specimen was corroded and pitted more severely than that in the RW specimen. However, numerous small cracks that could not be revealed by low-magnification microscope were found in the FZ.

3.3 Tensile Properties of A588 Steel Welds

Tensile properties of various specimens tested in both air and saturated H_2S solution are listed in Table 1. Because the hardness in the FZ was slightly higher than that in other regions of the welds, as shown in Fig. 3, it was expected that the ultimate tensile strength (UTS) of the steel plate would be lower than that of the welds in air. The results indicate that the fracture location of the RW specimen was in the BM. Therefore, the essential tensile properties of such a specimen were similar to those of the steel plate. In addition, the OW specimen consisted of outer surface layers of deposits and interior BM. Thus, it has the highest strength among the specimens tested in air. Regardless of the specimen type, excellent ductility was observed for all the specimens tested in air. However, all the specimens suffered severe degradation in tensile ductility when tested in a saturated H_2S solution. No apparent changes in strength were observed. Furthermore, the strength of the OW specimen exhibited significant variation in various environments, having the highest strength in air and lowest strength in a saturated H_2S solution among the specimens. It was also demonstrated that the fracture location of RW specimens changed from the BM in air to the FZ in a H_2S solution, suggesting that the FZ had a high susceptibility to HE.

When specimens were tested in a severely embrittling environment, most cracks were initiated at sites with high stress concentrations, *e.g.,* the corners of the rectangular tensile specimen. Figure 7 presents the macroscopic photographs of tensile-fractured specimens in a saturated H_2S solution. In the OW specimen, cracks initiated in the FZs and propagated into the interior BM (Fig. 7a). The HAZ, which is adjacent to the fusion boundaries has crack propagation normal to the loading direction, revealing a high sensitivity to HE. Tensile fracture of RW specimens (Fig. 7b) indicated that cracks originally initiated at the corners of the specimen and then propagated into the FZ. The final catastrophic failure resulted in the formation of significant plastic deformation in the BM underneath the FZ. In addition, the results also reveal that the weld interface was an easy crack path and that the BM was less susceptible to HE than the FZ and CGHAZ. Such results are also in agreement with the fact that the steel plate has a higher strength than either the RW or OW specimen in a saturated H_2S solution.

3.4 Fractographic Observations

The outer surface of U-bend specimens immersed in a saturated H_2S solution for 72 h examined by SEM is shown in Fig. 8. In the FZ, the columnar grain boundaries were more resistant to corrosion than the grain interior, as displayed in Fig. 8(a). The above-mentioned results also indicated that the FZ was more resistant to corrosion than the BM in the saturated H_2S solution. Thus, the highest resistance to corrosion was found in the columnar grain boundaries. However, microcracks were initiated and propagated along columnar grain boundaries (Fig. 8b). Such boundaries were associated with the microstructures of coarse elongated ferrite and Widmanstätten side plates (as shown in Fig. 4b). This is consistent with the previous report that microcracks induced by HE in the FZ would propagate along the columnar grain boundary ferrite with Widmanstätten

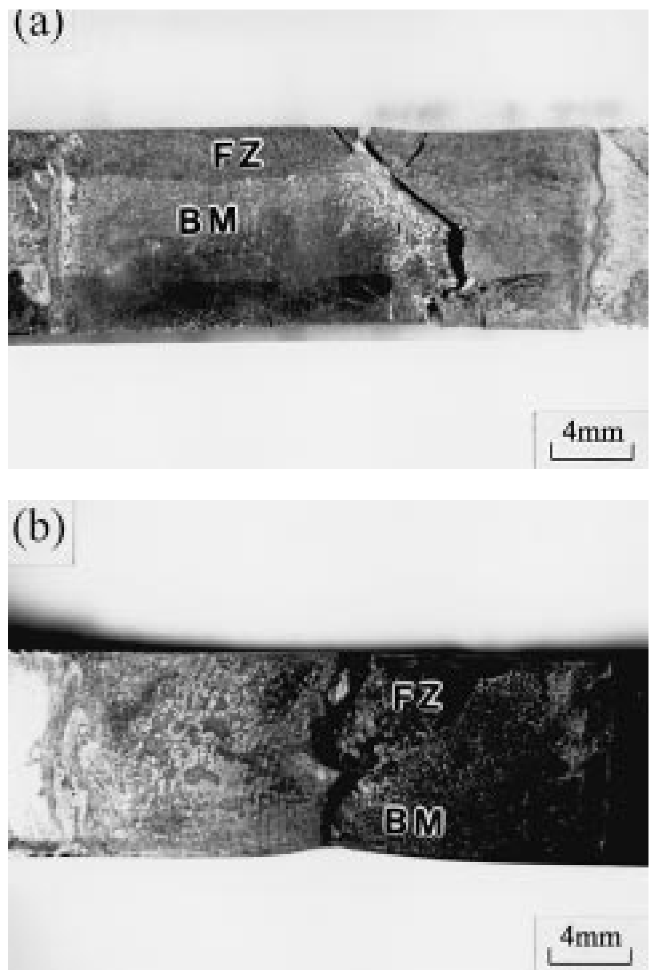

Fig. 7 Macroscopic photographs of tensile-fractured (**a**) OW and (**b**) RW specimens tested in a saturated H_2S solution

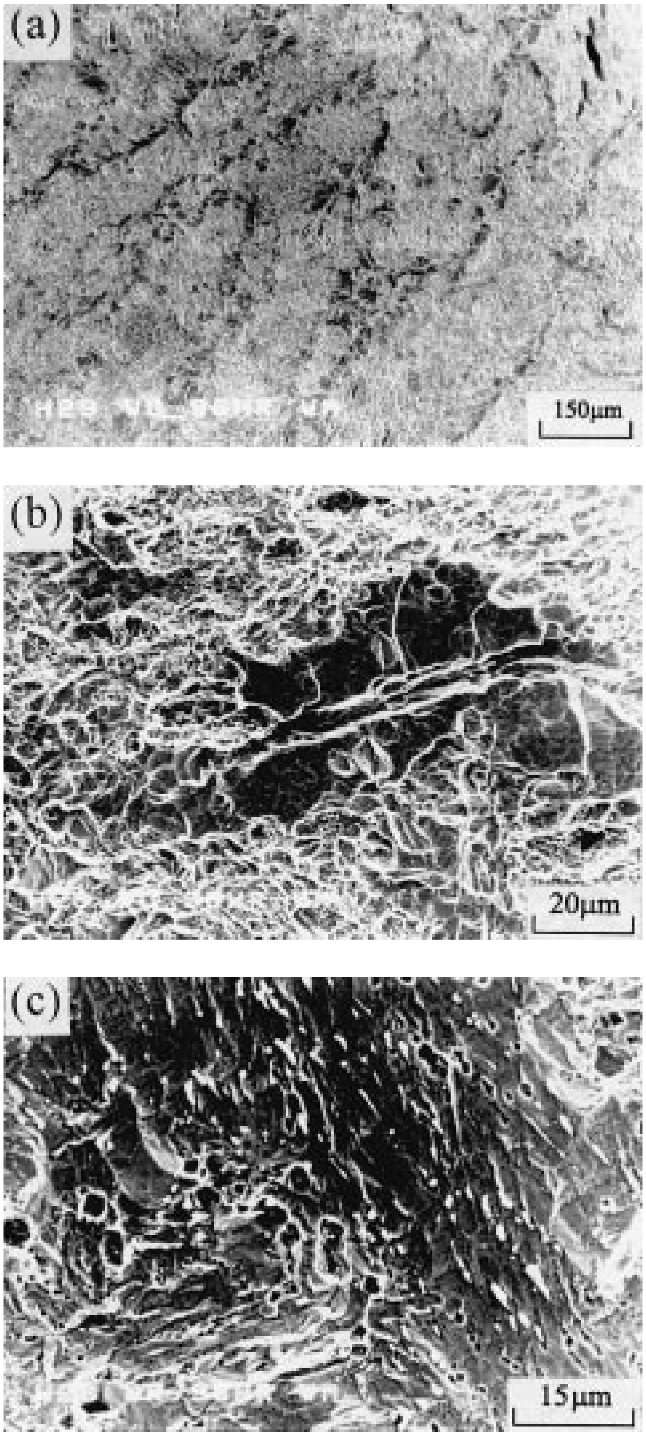

Fig. 8 SEM photographs of U-bend specimens in a saturated H_2S solution showing (**a**) the FZ, (**b**) microcracks in the columnar grain boundaries, and (**c**) the CGHAZ

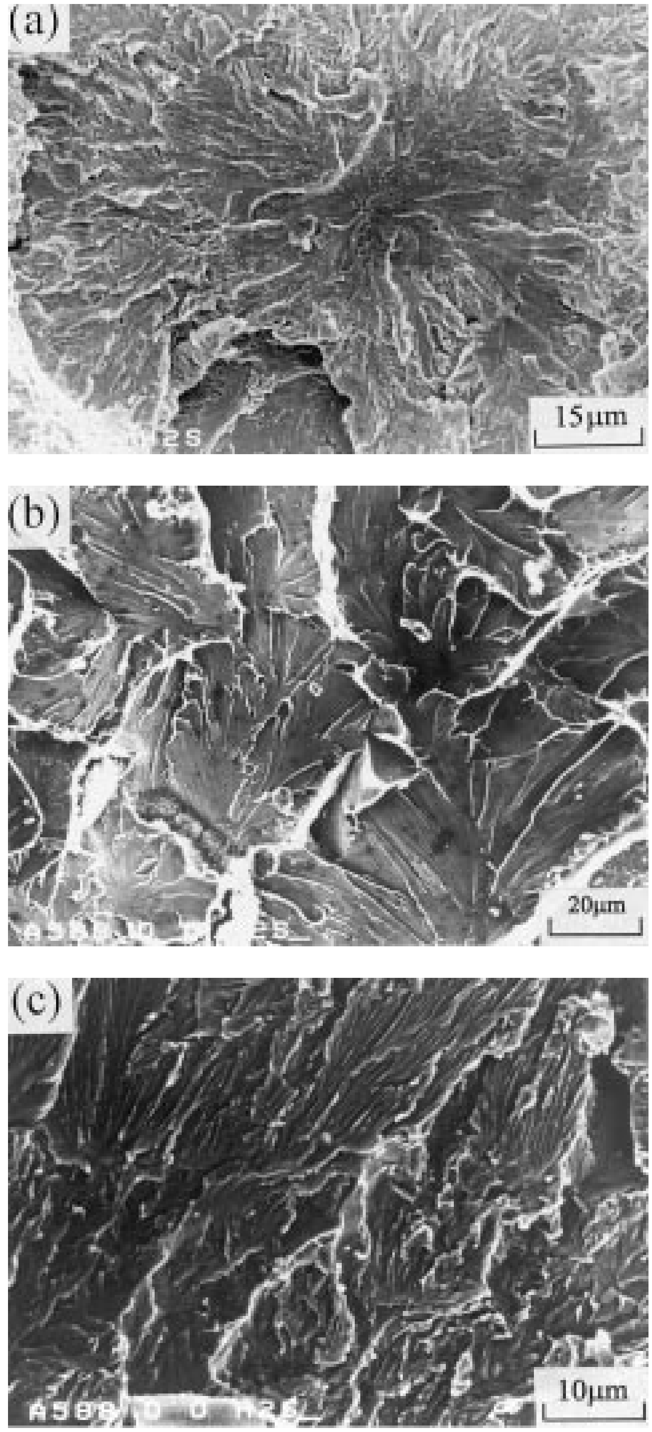

Fig. 9 SEM fractographs of tensile-fractured specimens tested in an H_2S solution showing (**a**) quasi-cleavage fracture in the steel plate, (**b**) cleavage fracture in the CGHAZ, and (**c**) featherlike fracture in the FZ of the weld

side plates and be arrested in the region of acicular ferrite.[22] In addition, it has been reported that the columnar grain boundary ferrite and associated side plates give rise to brittle fracture features.[22]

In current study, the initiation and coalescence of microcracks at those sites with susceptible microstructures occurred during SSRT tests, resulting in the degradation of tensile properties for the A588 steel welds in a saturated H_2S solution. Thus, it was expected that ferrite along coarse prior austenite boundaries and Widmanstätten side plates in the CGHAZ displaying somewhat brittle features (Fig. 8c). The weld toes associated with the microstructures of the CGHAZ had both the maximum stress and maximum strain due to the discontinuity of geometrical profile there. The accumulation of corrosive medium at the weld toes, together with susceptible microstructures, resulted in enhanced SSCC at those sites.

The excellent ductility of all the tensile specimens tested in air was associated with ductile dimple fracture. On the other hand, SEM fractographs of the tensile-fractured specimen in embrittling solution are shown in Fig. 9. The steel plate embrittled in a saturated H_2S solution revealed a quasi-cleavage fracture (Fig. 9a). It also showed that cleavage fracture occurred in the CGHAZ (Fig. 9b) and featherlike rupture occurred in the FZ revealing the metallurgical features of Widmanstätten side plates (Fig. 9c). All these brittle features are indications of HE. The nucleation and growth of microcracks along the columnar grain boundaries in the FZ were responsible for the deteriorated tensile properties of the OW specimen in the saturated H_2S solution. In this study, both U-bend and SSRT tests in a saturated H_2S solution revealed similar results, indicating that the coarse elongated ferrite and Widmanstätten side plates were susceptible to HE, causing premature failure of the A588 steel welds.

4. Conclusions

- A slight decrease in strength and a drastic drop in ductility were observed for A588 steel plate in a saturated H_2S solution as compared to those in air. The change in fracture location from the BM in air to the FZ in a saturated H_2S solution was observed for the RW specimen. Although the OW specimen exhibited the highest strength among specimens in air, its high susceptibility to HE of the deposits resulted in the severe degradation in tensile properties of this specimen in a saturated H_2S solution.
- The results of U-bend immersion tests revealed that the FZ had a higher corrosion resistance than the other regions of the weld in the sulfuric acid and the saturated H_2S solutions. The presence of a smaller anodic area (BM) in the OW specimen than in the RW specimen led to a more significant corrosion in the BM. The SEM photographs of U-bend specimens showed that columnar grain boundaries were more resistant to corrosion than the grain interior in the FZ. However, those boundaries had a high susceptibility to HE and induced microcracks. Reduced tensile properties of the OW specimens in a saturated H_2S solution could be related to the initiation and coalescence of numerous microcracks in the FZ along columnar grain boundaries during SSRT tests.
- Cleavage fracture in the CGHAZ and featherlike rupture in the FZ, revealing the metallurgical features of Widmanstätten side plates, were observed for welds tested in a saturated H_2S solution. The results also indicated that both FZ and CGHAZ were susceptible to HE.

Acknowledgments

The authors gratefully acknowledge the support of the Republic of China National Science Council (Contract No. NSC87-TPC-E-019-004). The authors are also indebted to Dr. S.D. Chyou, in Power Research Institute, for his valuable suggestions and assistance.

References

1. B.R. Meybaum, and E.S. Ayllon: *Corrosion,* 1980, vol. 36 (7), pp. 345-47.
2. M. Stratmann, K. Bohnenkamp, and T. Ramchandran: *Corr. Sci.,* 1987, vol. 27 (9), pp. 905-26.
3. S. Vaynman, R.S. Guico, M.E. Fine, and S.J. Manganello: *Metall. Mater. Trans. A,* 1997, vol. 28A, pp. 1274-76.
4. J.H. Wang, F.I. Wei, Y.S. Chang, and H.C. Shih: *Mater. Chem. Phys.,* 1997, vol. 47 (1), pp. 1-8.
5. H.C. Shih, J.C. Oung, J.T. Hsu, J.Y. Wu, and F.I. Wei: *Mater. Chem. Phys.,* 1994, vol. 37 (3), pp. 230-36.
6. J.B.Terrell, T.S. Sudarsham, and K.L. Rohr: *J. Heat Treatment,* 1987, vol. 5 (1), pp. 21-25.
7. P. Albrecht, and C. Shabshab: *Mater. Civ. Eng.,* 1994, vol. 6 (3), pp. 407-29.
8. J.M. Barsom, and B.G. Reisdorf: *WRC Bull.,* 1988, vol. 332, pp. 1-19.
9. C. Sheach and W.P. Tait: *Weld Metal Fabrication,* 1975, vol. 43 (10), pp. 747-55.
10. A.W. Pense: *WRC Bull.,* 1988, vol. 332, pp. 20-33.
11. C.V. Robino, R. Varughese, A.W. Pense, and R.C. Dias: *WRC Bull.,* 1988, vol. 330, pp. 1-10.
12. F. Mancia: *Corr. Sci.,* 1987, vol. 27 (10), pp. 1225-37.
13. G. Cragnolino, D.S. Dunn, and N. Sridhar: *Corrosion,* 1996, vol. 52 (3), pp. 194-203.
14. W. Yang, M. Zhang, G. Zhao, and J. Congleton: *Corrosion,* 1991, vol. 47 (4), pp. 226-33.
15. J.A. Beavers, and G.H. Koch: *Corrosion,* 1992, vol. 48 (3), pp. 256-64.
16. S. Maitra: *Corrosion,* 1981, vol. 37 (2), pp. 98-103.
17. Y. Yamaguchi, and H. Nonaka: *Corrosion,* 1994, vol. 50 (3), pp. 197-204.
18. R.N. Parkins: *Corrosion,* 1990, vol. 46 (3), pp. 178-89.
19. A. Ikeda, T. Kaneko, and Y. Ando: *Corr. Sci.,* 1987, vol. 27 (10), pp. 1099-15.
20. B.J. Berkowitz, and F.H. Heubaum: *Corrosion,* 1984, vol. 40 (5), pp. 240-45.
21. D.E. Hendrix: *Mater. Performance,* 1997, vol. 36 (12), pp. 54-56.
22. L.W. Tsay, C. Chen, and S.W. Cheng: *J. Chin. Inst. Eng.,* 1992, vol. 15 (3), pp. 285-92.